Local NMR relaxation rates T_1^{-1} and T_2^{-1} depending on the d-vector symmetry in the vortex state of chiral and helical p-wave superconductors

Kenta K. Tanaka,[1,*] Masanori Ichioka,[1,2,†] and Seiichiro Onari[1,2]
[1]*Department of Physics, Okayama University, Okayama 700-8530, Japan*
[2]*Research Institute for Interdisciplinary Science, Okayama University, Okayama 700-8530, Japan*

(Received 26 January 2018; published 10 April 2018)

Local NMR relaxation rates in the vortex state of chiral and helical p-wave superconductors are investigated by the quasiclassical Eilenberger theory. We calculate the spatial and resonance frequency dependences of the local NMR spin-lattice relaxation rate T_1^{-1} and spin-spin relaxation rate T_2^{-1}. Depending on the relation between the NMR relaxation direction and the d-vector symmetry, the local T_1^{-1} and T_2^{-1} in the vortex core region show different behaviors. When the NMR relaxation direction is parallel to the d-vector component, the local NMR relaxation rate is anomalously suppressed by the negative coherence effect due to the spin dependence of the odd-frequency s-wave spin-triplet Cooper pairs. The difference between the local T_1^{-1} and T_2^{-1} in the site-selective NMR measurement is expected to be a method to examine the d-vector symmetry of candidate materials for spin-triplet superconductors.

DOI: 10.1103/PhysRevB.97.134507

I. INTRODUCTION

The spin-triplet superconductors have attracted much attention since exotic states such as odd-frequency Cooper pairs and Majorana states are expected to be induced at the vortex core and surface regions. Although ruthenate superconductor Sr_2RuO_4, heavy fermion superconductor UPt_3, and other materials have been suggested as spin-triplet superconductors by many experimental and theoretical studies [1–6], the d-vector symmetries have not been identified. The d-vector symmetry was discussed to explain experimental observations such as magnetic field orientation dependences of the Knight shift [4,5] and the Pauli-limit behavior of H_{c2} [6]. In addition to these approaches, we need new methods to clarify the d-vector symmetry in the spin-triplet superconductors.

In the spin-triplet chiral p-wave superconductors, the theoretical studies for the local NMR spin-lattice relaxation rate T_1^{-1} revealed that the local T_1^{-1} in the vortex core region is anomalously suppressed [7–9]. The previous studies based on the Eilenberger theory found the site and resonance frequency dependences of T_1^{-1}, and the anomalous suppression of the local T_1^{-1} is derived from the negative coherence effect related to the odd-frequency s-wave spin-triplet Cooper pairs [10]. Experimentally, the local T_1^{-1} were detected by the site-selective NMR measurements for high-T_c superconductors [11–13] and the conventional superconductor [14]. As shown in Fig. 1(a), the local $T_1^{-1}(\boldsymbol{r})$ as a function of internal field $B(\boldsymbol{r})$ at the same position $\boldsymbol{r}$ can be observed by tuning the resonance frequency among the resonance line shape, since the internal field is in proportion to the resonance frequency. The spectrum of $B(\boldsymbol{r})$ in Sr_2RuO_4 is observed by μSR measurement [15].

In the uniform state of three-dimensional chiral superconductors with strong spin-orbit coupling and odd-parity pairing, significant suppression of the NMR relaxation rate is suggested for nuclear spins polarized along the nodal direction as a consequence of the spin-selective Majorana nature of nodal quasiparticles [16].

At the surface of the superfluid ^{3}He B phase, the odd-frequency s-wave spin-triplet Cooper pairs were studied in relation to the static spin susceptibility [17], and Ising-type spin relaxation was discussed in relation to the Majorana state [18]. In addition, a strong relation between the Majorana zero-energy mode and the odd-frequency Cooper pair has been revealed [19–22]. These spin-dependent surface states have information of the pairing symmetry, and are expected to be studied also in the vortex core states in spin-triplet superconductors. Since the NMR relaxation rate can prove the direction of the conduction electrons' spin, we expect that the d-vector structure in the vortex state is detected by site-selective NMR measurement with orientation control of the NMR relaxation direction. As shown in Fig. 1(b), for relaxation direction δM parallel (perpendicular) to the static applied field H, we observe the NMR spin-lattice relaxation rate T_1^{-1} (the NMR spin-spin relaxation rate T_2^{-1}) [23–25]. When applied fields H are along the z direction, T_1^{-1} by $\delta M \| \boldsymbol{z}$ comes from the xy component of dynamical spin susceptibility $\chi_{xx} + \chi_{yy}$. And T_2^{-1} is from $\chi_{zz} + \chi_{yy}$ if $\delta M \| \boldsymbol{x}$. Therefore, the difference between T_1^{-1} and T_2^{-1} may reflect the orientation of the d vector in spin-triplet superconductors.

In this paper, we study the local NMR relaxation rates T_1^{-1} and T_2^{-1} in the vortex state of chiral and helical p-wave superconductors. For chiral p-wave superconductors, we consider the two types of chiral p-wave states, $\boldsymbol{d} \| \boldsymbol{z}$ and $\boldsymbol{d} \| \boldsymbol{x}$, where the direction of the d vector indicates the z and x axis, respectively. In particular, we discuss how the relaxation rates depend on the direction of the NMR relaxation directions, calculating the site r and internal field B dependences of T_1^{-1}

*kktanaka@s.okayama-u.ac.jp
†ichioka@cc.okayama-u.ac.jp

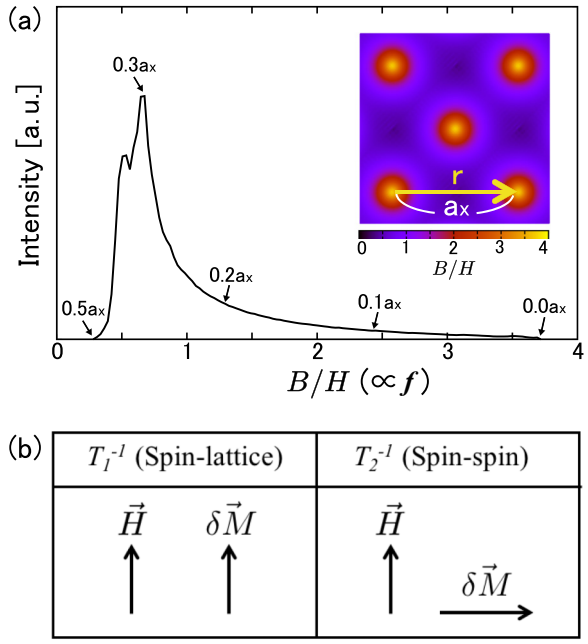

FIG. 1. (a) The Redfield pattern of the resonance line shape of the NMR, $P(B)$, for chiral p-wave pairing at $H/H_{c2} \simeq 0.023$ and $T/T_{c0} = 0.5$. The resonance line shape is derived from the distribution of the internal magnetic field $B(\boldsymbol{r})/H$ presented in the inset. $B(\boldsymbol{r})/H$ is in proportion to the resonance frequency f. In the inset, an arrow indicates radius r from the vortex center along the next-nearest-neighbor vortex direction. For example, the intensity at the maximum (minimum) $B(\boldsymbol{r})/H$ comes from the vortex center (midpoint) at the $r = 0.0a_x$ ($r = 0.5a_x$) region, and the peak intensity corresponds to the signal from the saddle point of the internal fields at the radius $r = 0.3a_x$ far from the vortex center. (b) Schematic picture of the relation between the NMR relaxation direction $\delta\vec{M}$ and the static field $\vec{H}$ in the cases of T_1^{-1} and T_2^{-1}.

and T_2^{-1}. These results help us to investigate the d-vector symmetry of chiral and helical p-wave superconductors by site-selective NMR measurement.

This paper is organized as follows. After the introduction, we describe our formulation of the quasiclassical Eilenberger equation in the vortex lattice state and the calculation method for the local NMR relaxation rates T_1^{-1} and T_2^{-1} in Sec. II. The derivations of T_1^{-1} and T_2^{-1} are explained in Appendix A based on the Eilenberger theory. In Sec. III, we investigate the site and B dependences of local T_1^{-1} and T_2^{-1} in the chiral and helical p-wave superconductors to find the relation to the d-vector symmetry. In Sec. IV and Appendix B, to understand the d-vector dependence, we discuss the site dependence of the coherence terms and the odd-frequency s-wave spin-triplet Cooper pairs around a vortex. The last section is devoted to the summary.

II. FORMULATION

We calculate the spatial structure of vortices in the vortex lattice state by quasiclassical Eilenberger theory. The quasiclassical theory is valid when the atomic scale is small enough compared to the superconducting coherence length. For many superconductors including Sr_2RuO_4, the quasiclassical condition is well satisfied.

For simplicity, we consider the chiral or the helical p-wave pairings on the two-dimensional cylindrical Fermi surface, $\boldsymbol{k} = (k_x, k_y) = k_F(\cos\theta_k, \sin\theta_k)$, and the Fermi velocity $\boldsymbol{v}_F = v_{F0}\boldsymbol{k}/k_F$. In the following, the hat symbol indicates the 2×2 matrix in spin space and the check symbol indicates the 4×4 matrix in particle-hole and spin spaces.

To obtain quasiclassical Green's functions $\check{g}(i\omega_n, \boldsymbol{r}, \boldsymbol{k})$ in the vortex lattice state, we solve the Riccati equation derived from the Eilenberger equation [26,27]

$$-i\boldsymbol{v}\cdot\nabla\check{g}(i\omega_n,\boldsymbol{r},\boldsymbol{k}) = \tfrac{1}{2}[i\tilde{\omega}_n\check{\tau}_3 - \check{\Delta}(\boldsymbol{r},\boldsymbol{k}), \check{g}(i\omega_n,\boldsymbol{r},\boldsymbol{k})] \quad (1)$$

in the clean limit, where $\boldsymbol{r}$ is the center-of-mass coordinate of the pair, $\boldsymbol{v} = \boldsymbol{v}_F/v_{F0}$, $\check{\tau}_3$ is the Pauli matrix defined in Eq. (A3), and $i\tilde{\omega}_n = i\omega_n - \boldsymbol{v}\cdot\boldsymbol{A}$ with Matsubara frequency ω_n. The quasiclassical Green's functions and order parameter are described by

$$\check{g}(i\omega_n,\boldsymbol{r},\boldsymbol{k}) = -i\pi\begin{bmatrix} \hat{g}(i\omega_n,\boldsymbol{r},\boldsymbol{k}) & i\hat{f}(i\omega_n,\boldsymbol{r},\boldsymbol{k}) \\ -i\hat{\bar{f}}(i\omega_n,\boldsymbol{r},\boldsymbol{k}) & -\hat{g}(i\omega_n,\boldsymbol{r},\boldsymbol{k}) \end{bmatrix}, \quad (2)$$

$$\check{\Delta}(\boldsymbol{r},\boldsymbol{k}) = \begin{bmatrix} 0 & \hat{\Delta}(\boldsymbol{r},\boldsymbol{k}) \\ -\hat{\Delta}^\dagger(\boldsymbol{r},\boldsymbol{k}) & 0 \end{bmatrix}, \quad (3)$$

where $\check{g}^2 = -\pi^2\check{1}$. The spin spaces of $\hat{g}$ and $\hat{\Delta}$ are, respectively, defined by the matrix elements

$$g_{\sigma\sigma'}(i\omega_n,\boldsymbol{r},\boldsymbol{k}) = \left[g_0(i\omega_n,\boldsymbol{r},\boldsymbol{k})\hat{1} + \sum_{\mu=x,y,z} g_\mu(i\omega_n,\boldsymbol{r},\boldsymbol{k})\hat{\sigma}_\mu\right]_{\sigma\sigma'}, \quad (4)$$

$$\Delta_{\sigma\sigma'}(\boldsymbol{r},\boldsymbol{k}) = \left[i\sum_{\mu=x,y,z}[d_\mu(\boldsymbol{r},\boldsymbol{k})\cdot\hat{\sigma}_\mu]\hat{\sigma}_y\right]_{\sigma\sigma'}, \quad (5)$$

where $\sigma,\sigma' = \uparrow$(up-spin) or $\downarrow$(down-spin), and d_μ is the μ component of the d vector. In addition, the matrix elements of the order parameter are defined by

$$\Delta_{\sigma\sigma'}(\boldsymbol{r},\boldsymbol{k}) = \Delta_{+,\sigma\sigma'}(\boldsymbol{r})\phi_{p+}(\boldsymbol{k}) + \Delta_{-,\sigma\sigma'}(\boldsymbol{r})\phi_{p-}(\boldsymbol{k}) \quad (6)$$

with the order parameter $\Delta_{\pm,\sigma\sigma'}(\boldsymbol{r})$ and the pairing function $\phi_{p\pm}(\boldsymbol{k}) = k_x \pm ik_y$ for the $p_\pm$ state.

Length, temperature, and magnetic field are, respectively, measured in units of ξ_0, T_{c0}, and B_0. Here, $\xi_0 = \hbar v_{F0}/2\pi k_B T_{c0}$ and $B_0 = \phi_0/2\pi\xi_0^2$ with the flux quantum ϕ_0. T_{c0} is the superconducting transition temperature at a zero magnetic field. The energy E, pair potential Δ, and ω_n are in units of $\pi k_B T_{c0}$. In the following, we set $\hbar = k_B = 1$. In this paper, our calculations are performed at $H/B_0 = 0.02$ and $T = 0.5T_{c0}$. In the chiral p-wave and helical p-wave states at $T = 0.5T_{c0}$, the upper critical fields $H_{c2}/B_0 \simeq 0.85$.

We set the magnetic field along the z axis, where the vector potential $\boldsymbol{A}(\boldsymbol{r}) = \frac{1}{2}\boldsymbol{H}\times\boldsymbol{r} + \boldsymbol{a}(\boldsymbol{r})$ in the symmetric gauge. $\boldsymbol{H} = (0,0,H)$ is a uniform flux density, and $\boldsymbol{a}(\boldsymbol{r})$ is related to the internal field $\boldsymbol{B}(\boldsymbol{r}) = (0,0,B(\boldsymbol{r})) = \boldsymbol{H} + \nabla\times\boldsymbol{a}(\boldsymbol{r})$. The unit cell of the vortex lattice is set as a square lattice [1]. From the distribution of $B(\boldsymbol{r})$, we calculate the resonance line shape called the Redfield pattern given by $P(B) = \int\delta[B - B(\boldsymbol{r})]d\boldsymbol{r}$ in Fig. 1.

To determine the pair potential $\hat{\Delta}(\boldsymbol{r})$ and the quasiclassical Green's functions self-consistently, we calculate the order parameter $\hat{\Delta}_{\pm}(\boldsymbol{r})$ by the gap equation

$$\hat{\Delta}_{\pm}(\boldsymbol{r}) = gN_0T \sum_{|\omega_n|\leqslant\omega_{\rm cut}} \langle \phi^*_{p\pm}(\boldsymbol{k})\hat{f}(i\omega_n,\boldsymbol{r},\boldsymbol{k})\rangle_{\boldsymbol{k}}, \tag{7}$$

where $\langle\ldots\rangle_{\boldsymbol{k}}$ indicates Fermi-surface average, $(gN_0)^{-1} = \ln T + 2T\sum_{0<\omega_n\leqslant\omega_{\rm cut}}\omega_n^{-1}$, and we use $\omega_{\rm cut} = 20k_{\rm B}T_{\rm c0}$. In Eq. (7), p-wave pairing interaction is isotropic in spin space. For the self-consistent calculation of the vector potential for the internal field $B(\boldsymbol{r})$, we use the current equation

$$\nabla\times(\nabla\times\boldsymbol{A}) = -\frac{2T}{\kappa^2}\sum_{0<\omega_n}\langle \boldsymbol{v}{\rm Im}\{g_0\}\rangle_{\boldsymbol{k}} \tag{8}$$

with the Ginzburg-Landau parameter $\kappa = B_0/\pi k_{\rm B}T_{\rm c}\sqrt{8\pi N_0}$. In our calculations, we use $\kappa = 2.7$ appropriate to Sr_2RuO_4 as a candidate material for the chiral or helical p-wave superconductor. The results of this paper are not changed qualitatively by the choice of the Ginzburg-Landau parameter as long as a type-II superconducting vortex state is maintained. We iterate calculations of Eqs. (1), (7), and (8) for ω_n until we obtain the self-consistent results of $\boldsymbol{A}(\boldsymbol{r})$, $\hat{\Delta}(\boldsymbol{r},\boldsymbol{k})$, and the quasiclassical Green's functions in the vortex lattice state.

In the chiral p-wave superconductors, we only consider the p_- state, i.e., antiparallel vortex state, since the antiparallel vortex state is stable compared to the parallel vortex state [28,29]. For variety of d-vector orientation, we calculate two types of chiral p-wave states, $\boldsymbol{d}\|z$ and $\boldsymbol{d}\|\boldsymbol{x}$, which are, respectively, defined by $\boldsymbol{d}(\boldsymbol{k}) \propto (k_x - ik_y)\hat{z}$ and $(k_x - ik_y)\hat{x}$. In the helical p-wave superconductors, we set the d vector as $\boldsymbol{d}(\boldsymbol{k}) \propto k_x\hat{x} + k_y\hat{y} = \phi_{p_+}(\boldsymbol{k})\boldsymbol{d}_- + \phi_{p_-}(\boldsymbol{k})\boldsymbol{d}_+$ in the uniform state at zero field, with $\boldsymbol{d}_{\pm}(\boldsymbol{k}) = \frac{1}{2}(1,\pm{\rm i},0)$. Thus, when we iterate calculations of Eqs. (1), (7), and (8), as an initial value, the d vector is set to be $\boldsymbol{d}(\boldsymbol{r},\boldsymbol{k}) = \Psi(\boldsymbol{r})\boldsymbol{d}(\boldsymbol{k})$ where $\Psi(\boldsymbol{r})$ is the Abrikosov vortex lattice solution.

Next, using the self-consistently obtained $\boldsymbol{A}(\boldsymbol{r})$ and $\hat{\Delta}(\boldsymbol{r})$, we calculate $\check{g}({\rm i}\omega_n,\boldsymbol{r},\boldsymbol{k})|_{{\rm i}\omega_n\to E\pm i\eta}$ for real energy E by solving Eilenberger Eq. (1) with $i\omega_n \to E \pm i\eta$. In this paper, we define the retarded and advanced Green's functions $\check{g}^R(E,\boldsymbol{r},\boldsymbol{k}) = \check{g}({\rm i}\omega_n,\boldsymbol{r},\boldsymbol{k})|_{{\rm i}\omega_n\to E+i\eta}$ and $\check{g}^A(E,\boldsymbol{r},\boldsymbol{k}) = \check{g}({\rm i}\omega_n,\boldsymbol{r},\boldsymbol{k})|_{{\rm i}\omega_n\to E-i\eta}$, respectively. η is a small parameter, and we use $\eta = 0.01$. We use the components of $\check{g}^R(E,\boldsymbol{r},\boldsymbol{k})$ and $\check{g}^A(E,\boldsymbol{r},\boldsymbol{k})$ to numerically calculate local $(T_1T)^{-1}$ and $(T_2T)^{-1}$ in the vortex lattice state.

A. NMR spin-lattice relaxation rate T_1^{-1}

We consider the conventional form of the local hyperfine fields from the conduction electrons [24]. Therefore, relaxation rates T_1^{-1} and T_2^{-1} of the nuclear magnetization are affected by the dynamical spin susceptibility of the local electronic state, which reflects spin states of the odd-frequency s-wave spin-triplet Cooper pairs at the atomic site in the vortex core region, as discussed later.

The NMR spin-lattice relaxation rate T_1^{-1} by $\delta M \parallel \boldsymbol{z}$ is calculated from xy components of dynamical spin susceptibility, $\chi_{xx} + \chi_{yy} \propto \chi_{-+}$, Therefore, as described in Appendix A following Refs. [8,10], T_1^{-1} is given by

$$\frac{[T_1(T)T]^{-1}}{[T_1(T_c)T_c]^{-1}} = \frac{\left[T_1^{gg}(T)T\right]^{-1} + \left[T_1^{ff}(T)T\right]^{-1}}{[T_1(T_c)T_c]^{-1}} = \int_{-\infty}^{\infty}\frac{W_{\rm sl}^{gg}(E,\boldsymbol{r}) + W_{\rm sl}^{ff}(E,\boldsymbol{r})}{4T\cosh^2(E/2T)}dE, \tag{9}$$

where

$$W_{\rm sl}^{gg}(E,\boldsymbol{r}) = \langle a_{\downarrow\downarrow}^{22}(E,\boldsymbol{r},\boldsymbol{k})\rangle_{\boldsymbol{k}}\langle a_{\uparrow\uparrow}^{11}(-E,\boldsymbol{r},\boldsymbol{k})\rangle_{\boldsymbol{k}}, \tag{10}$$

$$W_{\rm sl}^{ff}(E,\boldsymbol{r}) = -\langle a_{\downarrow\uparrow}^{21}(E,\boldsymbol{r},\boldsymbol{k})\rangle_{\boldsymbol{k}}\langle a_{\uparrow\downarrow}^{12}(-E,\boldsymbol{r},\boldsymbol{k})\rangle_{\boldsymbol{k}} \tag{11}$$

with

$$\begin{aligned} a_{\sigma\sigma'}^{11}(E,\boldsymbol{r},\boldsymbol{k}) &= \frac{1}{2}\left[g_{\sigma\sigma'}^R(E,\boldsymbol{r},\boldsymbol{k}) - g_{\sigma\sigma'}^A(E,\boldsymbol{r},\boldsymbol{k})\right],\\ a_{\sigma\sigma'}^{22}(E,\boldsymbol{r},\boldsymbol{k}) &= \frac{1}{2}\left[\bar{g}_{\sigma\sigma'}^R(E,\boldsymbol{r},\boldsymbol{k}) - \bar{g}_{\sigma\sigma'}^A(E,\boldsymbol{r},\boldsymbol{k})\right],\\ a_{\sigma\sigma'}^{12}(E,\boldsymbol{r},\boldsymbol{k}) &= \frac{i}{2}\left[f_{\sigma\sigma'}^R(E,\boldsymbol{r},\boldsymbol{k}) - f_{\sigma\sigma'}^A(E,\boldsymbol{r},\boldsymbol{k})\right],\\ a_{\sigma\sigma'}^{21}(E,\boldsymbol{r},\boldsymbol{k}) &= \frac{i}{2}\left[\bar{f}_{\sigma\sigma'}^R(E,\boldsymbol{r},\boldsymbol{k}) - \bar{f}_{\sigma\sigma'}^A(E,\boldsymbol{r},\boldsymbol{k})\right], \end{aligned} \tag{12}$$

where $\sigma,\sigma' = \uparrow$(up-spin) or $\downarrow$(down-spin). $T_c(<T_{\rm c0})$ is superconducting transition temperature at a finite magnetic field, and $\hat{\bar{g}}^R(E,\boldsymbol{r},\boldsymbol{k}) = \hat{g}^R(-E,\boldsymbol{r},\boldsymbol{k})$. In Eq. (9), $(T_1T)^{-1}$ is divided into two contributions, the density of state (DOS) term $(T_1^{gg}T)^{-1}$ from $W_{\rm sl}^{gg}$ and the coherence term $(T_1^{ff}T)^{-1}$ from $W_{\rm sl}^{ff}$.

B. NMR spin-spin relaxation rate T_2^{-1}

From the field theory of NMR relaxation rate [24], we derive the NMR spin-spin relaxation rate T_2^{-1} by $\delta M \parallel \boldsymbol{x}$ from the dynamical spin susceptibility $\chi_{yy} + \chi_{zz}$, based on the Eilenberger theory. Since χ_{yy} gives $\frac{1}{2}T_1^{-1}$, T_2^{-1} is given in the form

$$T_2^{-1} = \tfrac{1}{2}T_1^{-1} + \tfrac{1}{2}T_{2zz}^{-1}, \tag{13}$$

where $\frac{1}{2}T_{2zz}^{-1}$ is the contribution from χ_{zz}. In the following, we focus on T_{2zz}^{-1} instead of T_2^{-1}.

As described in Appendix A, T_{2zz}^{-1} is given by

$$\frac{1}{2}\frac{[T_{2zz}(T)T]^{-1}}{[T_{2zz}(T_c)T_c]^{-1}} = \frac{1}{2}\frac{\left[T_{2zz}^{gg}(T)T\right]^{-1} + \left[T_{2zz}^{ff}(T)T\right]^{-1}}{[T_{2zz}(T_c)T_c]^{-1}} = \sum_{\sigma\sigma'}S_{\sigma\sigma'}\int_{-\infty}^{\infty}\frac{W_{\sigma\sigma'}^{gg}(E,\boldsymbol{r}) + W_{\sigma\sigma'}^{ff}(E,\boldsymbol{r})}{16T\cosh^2(E/2T)}dE, \tag{14}$$

where

$$W_{\sigma\sigma'}^{gg}(E,\boldsymbol{r}) = \left\langle a_{\sigma\sigma'}^{22}(E,\boldsymbol{r},\boldsymbol{k})\right\rangle_{\boldsymbol{k}}\left\langle a_{\sigma\sigma'}^{11}(-E,\boldsymbol{r},\boldsymbol{k})\right\rangle_{\boldsymbol{k}}, \tag{15}$$

$$W_{\sigma\sigma'}^{ff}(E,\boldsymbol{r}) = -\left\langle a_{\sigma\sigma'}^{21}(E,\boldsymbol{r},\boldsymbol{k})\right\rangle_{\boldsymbol{k}}\left\langle a_{\sigma\sigma'}^{12}(-E,\boldsymbol{r},\boldsymbol{k})\right\rangle_{\boldsymbol{k}}, \tag{16}$$

$S_{\sigma\sigma'} = 1$ when $\sigma = \sigma'$, and $S_{\sigma\sigma'} = -1$ when $\sigma\neq\sigma'$. Also in Eq. (14), $(T_{2zz}T)^{-1}$ is divided into two contributions of the DOS term $(T_{2zz}^{gg}T)^{-1}$ from $W_{\sigma\sigma'}^{gg}$ and the coherence term $(T_{2zz}^{ff}T)^{-1}$ from $W_{\sigma\sigma'}^{ff}$.

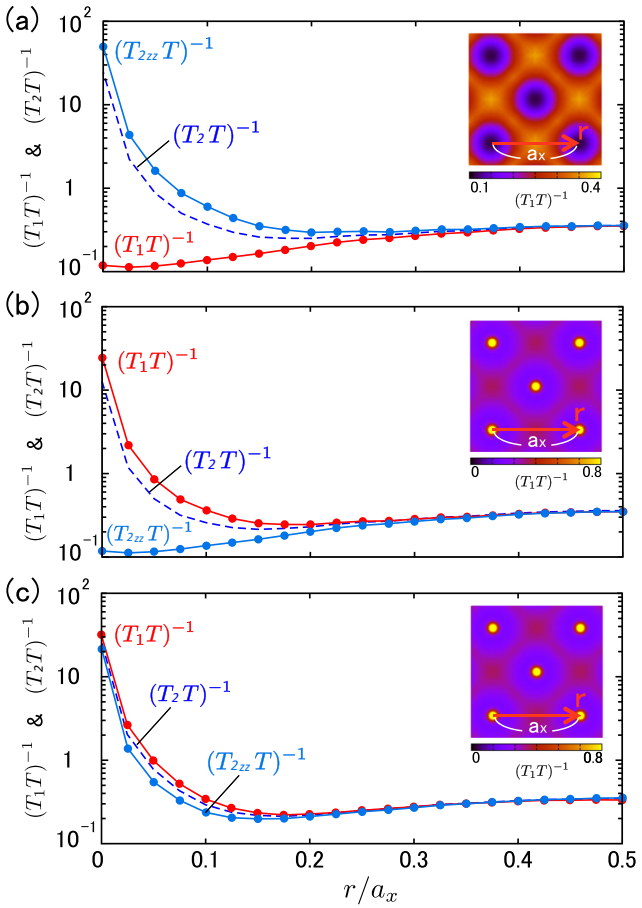

FIG. 2. r dependence of $(T_1T)^{-1}$ and $(T_{2zz}T)^{-1}$ in (a) the chiral p-wave $\boldsymbol{d}\|\boldsymbol{z}$, (b) the chiral p-wave $\boldsymbol{d}\|\boldsymbol{x}$, and (c) the helical p-wave states. The dashed lines are for $(T_2T)^{-1} = (T_1T)^{-1}/2 + (T_{2zz}T)^{-1}/2$. The insets show the spatial distribution of $(T_1T)^{-1}$ in each state. $H/H_{c2} \simeq 0.023$ and $T/T_{c0} = 0.5$.

In the spin-singlet pairing state and the normal state, $T_1^{-1} = T_2^{-1} = T_{2zz}^{-1}$, since $\sum_{\sigma\sigma'} W_{\sigma\sigma'}^{gg} = 2W_{\rm sl}^{gg}$ and $\sum_{\sigma\sigma'} W_{\sigma\sigma'}^{ff} = 2W_{\rm sl}^{ff}$.

III. SITE AND INTERNAL FIELD DEPENDENCES OF LOCAL NMR RELAXATION RATES

First, we study the local NMR relaxation rates $[T_1(r)T]^{-1}$, $[T_2(r)T]^{-1}$, and $[T_{2zz}(r)T]^{-1}$ as a function of radius r on a line between next-nearest-neighbor (NNN) vortices in the vortex state of chiral and helical p-wave superconductors. The results are presented in Fig. 2. At the outside of the vortex core region $r/a_x > 0.25$, the difference between $(T_1T)^{-1}$ and $(T_{2zz}T)^{-1}$ is very small in all pairing cases in Fig. 2. Therefore, we cannot obtain information about the d-vector symmetry from the observation of $(T_1T)^{-1}$ and $(T_2T)^{-1}$ in the uniform superconductivity outside of vortex cores.

On the other hand, in the vortex core region $r/a_x < 0.25$, we can see the obvious difference between $(T_1T)^{-1}$ and $(T_{2zz}T)^{-1}$. In Fig. 2(a) for the chiral p-wave $\boldsymbol{d}\|\boldsymbol{z}$ state, $(T_1T)^{-1}$ shows the anomalous suppression of the relaxation rate around the vortex core [10], but $(T_{2zz}T)^{-1}$ shows enhancement at the vortex core. The enhancement reflects the accumulation of low-energy quasiparticles around the vortex core. In Fig. 2(b) for the chiral p-wave $\boldsymbol{d}\|\boldsymbol{x}$ state, at the vortex core $(T_{2zz}T)^{-1}$ shows the anomalous suppression, and $(T_1T)^{-1}$ shows the enhancement. From the differences between Figs. 2(a) and 2(b), we realize that the suppression of the relaxation rate occurs when the d vector is parallel to the NMR relaxation direction δM. Therefore, we can extract information about the d-vector orientation from comparative observation of T_1^{-1} and T_2^{-1} at the vortex core region in the site-selective NMR measurement.

In Fig. 2(c) for the helical p-wave state, the r dependences of $(T_1T)^{-1}$ and $(T_{2zz}T)^{-1}$ show similar enhancement at the vortex core, but $(T_{2zz}T)^{-1}$ is smaller than $(T_1T)^{-1}$ in the vortex core. This is because the d vector in the helical p-wave pairing is within the xy plane, and some components of the d vector parallel to $\delta M(\| \boldsymbol{x})$ partially contribute to the suppression of $(T_{2zz}T)^{-1}$.

Next, we study the internal field B dependence of local $(T_1T)^{-1}$ and $(T_{2zz}T)^{-1}$ in the vortex state of chiral and helical p-wave superconductors to discuss how the difference between T_1^{-1} and T_2^{-1} for each d-vector symmetry is detected in the site-selective NMR measurement. As presented in Fig. 3, the local $[T_1(\boldsymbol{r})T]^{-1}$ is plotted as a function of $B(\boldsymbol{r})$ at the same position $\boldsymbol{r}$. The signal from the higher (lower) field comes from inside (outside) of the vortex core. In Fig. 3(a) for the chiral p-wave $\boldsymbol{d}\|\boldsymbol{z}$ state, $(T_1T)^{-1}$ shows monotonically decreasing behavior as a function of B. $(T_{2zz}T)^{-1}$ shows also decreasing behavior in the range $B \lesssim 1$, but in high-field ranges $(T_{2zz}T)^{-1}$ shows increasing behavior towards a large value at the vortex center. In Fig. 3(b) for the chiral p-wave $\boldsymbol{d}\|\boldsymbol{x}$ state, $(T_{2zz}T)^{-1}$ shows similar monotonic decreasing behavior to those of $(T_1T)^{-1}$ in Fig. 3(a). On the other hand, $(T_1T)^{-1}$ in Fig. 3(b) shows similar enhancement at the vortex core but the magnitude is smaller, compared to that of $(T_{2zz}T)^{-1}$ in Fig. 3(a). In Fig. 3(c) for the helical p-wave state, $(T_1T)^{-1}$ and $(T_{2zz}T)^{-1}$ show decreasing behavior as a function of B in the range $B \lesssim 1.5$, but these relaxation rates show increasing behavior in high-field ranges. The magnitude of $(T_{2zz}T)^{-1}$ is about half of $(T_1T)^{-1}$.

Therefore, the NMR relaxation rates show different behavior between $(T_1T)^{-1}$ and $(T_{2zz}T)^{-1}$ at the vortex core region in chiral p-wave $\boldsymbol{d}\|\boldsymbol{z}$, chiral p-wave $\boldsymbol{d}\|\boldsymbol{x}$, and helical p-wave states. The reason for this difference is related to the negative coherence effect and the odd-frequency spin-triplet Cooper pairs around the vortex center, as discussed in the next section.

IV. NEGATIVE COHERENCE EFFECT AND ODD-FREQUENCY s-WAVE SPIN-TRIPLET COOPER PAIRS

To discuss the reason for the differences in anomalous suppressions of the NMR relaxation rates between cases presented in Figs. 2 and 3, we show the site dependence of the coherence terms $(T_1^{ff}T)^{-1}$ and $(T_{2zz}^{ff}T)^{-1}$ with the DOS term $(T_1^{gg}T)^{-1}$, and the amplitudes of odd-frequency s-wave spin-triplet Cooper pairs around the vortex core in the chiral and helical p-wave superconductors. The results are presented in Fig. 4 along the NNN direction, and summarized in Table I. We note that the local NMR relaxation rate is divided into two

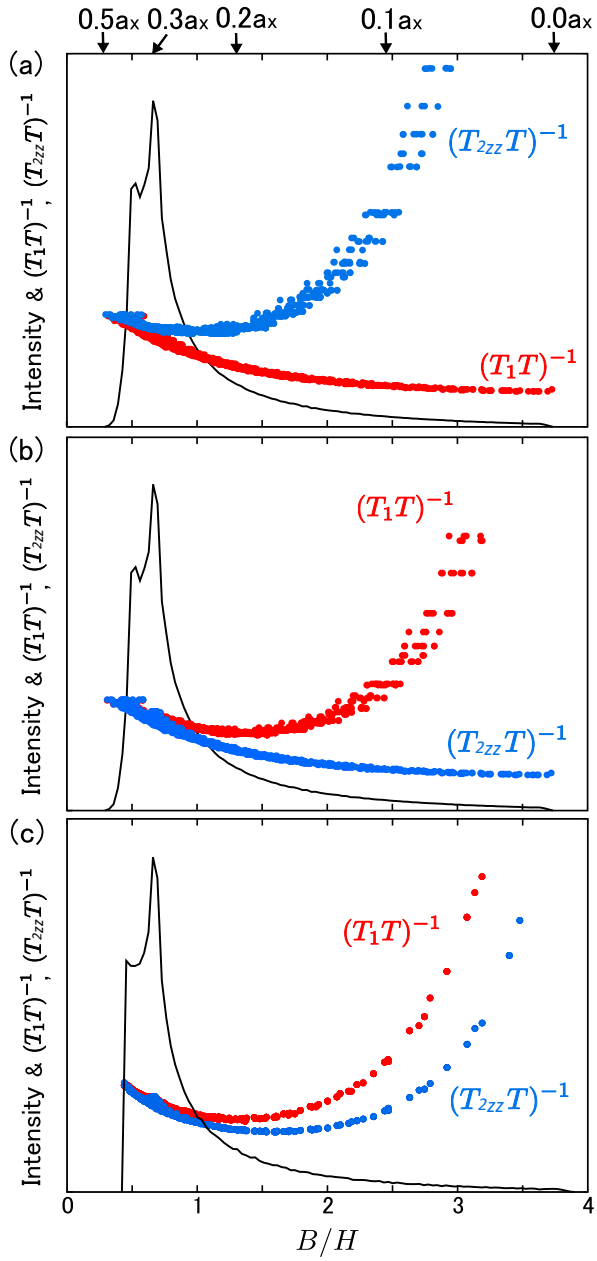

FIG. 3. Points are for the B dependence of $(T_1T)^{-1}$ and $(T_{2zz}T)^{-1}$ in (a) the chiral p-wave $\boldsymbol{d}\|\boldsymbol{z}$, (b) the chiral p-wave $\boldsymbol{d}\|\boldsymbol{x}$, and (c) the helical p-wave states, corresponding to the cases in Fig. 2. Only data points for $(T_1T)^{-1} \leqslant 1.2$ are presented. $H/H_{c2} \simeq 0.023$ and $T/T_{c0} = 0.5$. In (a), (b), and (c), solid line indicates the Redfield pattern of the resonance line shape $P(B)$ in Fig. 1(a) for the chiral p-wave $\boldsymbol{d}\|\boldsymbol{z}$ and $\boldsymbol{d}\|\boldsymbol{x}$ states and helical p-wave states, respectively. These are almost on the same line.

contributions of the DOS term and the coherence term so that $1/T_{1(2zz)} = 1/T_{1(2zz)}^{gg} + 1/T_{1(2zz)}^{ff}$

As shown by a black solid line in Fig. 4(a) for the chiral p-wave $\boldsymbol{d}\|\boldsymbol{z}$ state, the DOS term $(T_1^{gg}T)^{-1}$ is enhanced with approaching the vortex center, because $(T_1^{gg}T)^{-1}$ reflects the low-energy local DOS of bound states around the vortex. We note that $(T_1^{gg}T)^{-1}$ is a small but finite value even at the outside, $r/a_x \sim 0.2$, since the bound states have small tails extending toward the outside of the vortex core. The r dependences of $(T_1^{gg}T)^{-1}$ and $(T_{2zz}^{gg}T)^{-1}$ show similar behavior also for the chiral p-wave $\boldsymbol{d}\|\boldsymbol{x}$ state and the helical p-wave state.

Compared to $(T_1^{gg}T)^{-1}$ and $(T_{2zz}^{gg}T)^{-1}$, contributions of the coherence terms $(T_1^{ff}T)^{-1}$ and $(T_{2zz}^{ff}T)^{-1}$ in Fig. 4(a) are negligible in the outside region of the vortex core, but become comparative contributions with approaching the vortex center. For the chiral p-wave $\boldsymbol{d}\|\boldsymbol{z}$ state, $(T_1^{ff}T)^{-1}$ is negative and $(T_{2zz}^{ff}T)^{-1}$ is positive. The former negative contributions are the origin of the anomalous suppression of $(T_1T)^{-1}$ at the vortex core [10], and the latter further enhances $(T_{2zz}T)^{-1}$ at the vortex core. Their magnitudes satisfy $|(T_1^{ff}T)^{-1}| \sim |(T_{2zz}^{ff}T)^{-1}|$ in the whole range of r in Fig. 4(a). At the vortex center, $(T_1^{ff}T)^{-1} \sim -(T_1^{gg}T)^{-1} \sim -24.7$.

For the chiral p-wave $\boldsymbol{d}\|\boldsymbol{x}$ state, the r dependence of $(T_{2zz}^{ff}T)^{-1}$ is the same as $(T_1^{ff}T)^{-1}$ in the chiral p-wave $\boldsymbol{d}\|\boldsymbol{z}$ state. At the vortex center, $(T_{2zz}^{ff}T)^{-1} \sim -(T_{2zz}^{gg}T)^{-1} \sim -24.7$. Therefore, $(T_{2zz}T)^{-1}$ in the $\boldsymbol{d}\|\boldsymbol{x}$ state shows similar anomalous suppression at the vortex core to those of $(T_1T)^{-1}$ in the $\boldsymbol{d}\|\boldsymbol{z}$ state. The anomalous suppression at the vortex core occurs when the NMR relaxation direction $\delta\boldsymbol{M}\|\boldsymbol{d}$. On the other hand, $(T_1^{ff}T)^{-1} = 0$ in the $\boldsymbol{d}\|\boldsymbol{x}$ state. Since the enhancement by $(T_1^{ff}T)^{-1}$ does not work, $(T_1T)^{-1}$ in Fig. 3(b) is smaller than $(T_{2zz}T)^{-1}$ in Fig. 3(a).

For the helical p-wave state with $\boldsymbol{d}\|xy$, $(T_1^{ff}T)^{-1} = 0$, and $(T_{2zz}^{ff}T)^{-1} \sim \frac{1}{2}(T_{2zz}^{gg}T)^{-1}$. This is because of the similar situation as in the chiral p-wave $\boldsymbol{d}\|\boldsymbol{x}$ state. However, since only part of the d vector is parallel to δM, near the vortex center $-(T_{2zz}^{ff}T)^{-1}$ is smaller than that of the $\boldsymbol{d}\|\boldsymbol{x}$ state. At the vortex center, $|(T_{2zz}^{ff}T)^{-1}| \sim 12.3$ in the helical p-wave state.

In the relations $(T_1^{ff}T)^{-1} \sim -(T_1^{gg}T)^{-1}$ for the chiral p-wave $\boldsymbol{d}\|\boldsymbol{z}$ state, there are small deviations between them in our numerical calculation at finite temperature. However, as discussed in Appendix B, in the limit $T \to 0$ we expect $(T_1^{ff}T)^{-1} \to -(T_1^{gg}T)^{-1}$ so that $(T_1T)^{-1} \to 0$. This is also expected for the relations $(T_{2zz}^{ff}T)^{-1} \sim -(T_{2zz}^{gg}T)^{-1}$ for the chiral p-wave $\boldsymbol{d}\|\boldsymbol{x}$ state.

In the previous study for the local T_1^{-1} in the chiral p-wave $\boldsymbol{d}\|\boldsymbol{z}$ state [10], it is revealed that the negative coherence term $(T_1^{ff}T)^{-1}$, inducing the anomalous suppression of $(T_1T)^{-1}$ around the vortex core, is related to the odd-frequency s-wave spin-triplet Cooper pair $\mathcal{F}_s(E=0,\boldsymbol{r})$. In addition, we found that $[T_1^{ff}(\boldsymbol{r})T]^{-1} = -|\mathcal{F}_s(E=0,\boldsymbol{r})|^2$ in the low-energy limit at low T and the limit of the isolated vortex at low fields H, and the negative coherence term $[T_1^{ff}(\boldsymbol{r})T]^{-1}$ tends to cancel the local DOS term $[T_1^{gg}(\boldsymbol{r})T]^{-1} = N(E=0,\boldsymbol{r})^2$, where $N(E=0,\boldsymbol{r})$ is the local DOS. A previous study using the Bogoliubov–de Gennes theory revealed the relation $N(E=0,\boldsymbol{r}) \propto |\mathcal{F}_{s,\uparrow\downarrow}(E=0,\boldsymbol{r})|$ in the chiral p-wave $\boldsymbol{d}\|\boldsymbol{z}$ state for the vortex core quasiparticle states with Majorana zero-energy mode [30].

The spin-resolved local DOS $N_\sigma(E,\boldsymbol{r})$ is given by

$$N_\sigma(E,\boldsymbol{r}) = \left\langle \mathrm{Re}\left[g_{\sigma\sigma}^R(E,\boldsymbol{r},\boldsymbol{k})\right]\right\rangle_{\boldsymbol{k}}. \tag{17}$$

where $\sigma = \uparrow$ or $\downarrow$ [27]. The local DOS is defined as $2N(E,\boldsymbol{r}) = N_\downarrow(E,\boldsymbol{r}) + N_\uparrow(E,\boldsymbol{r})$. And the spin-dependent

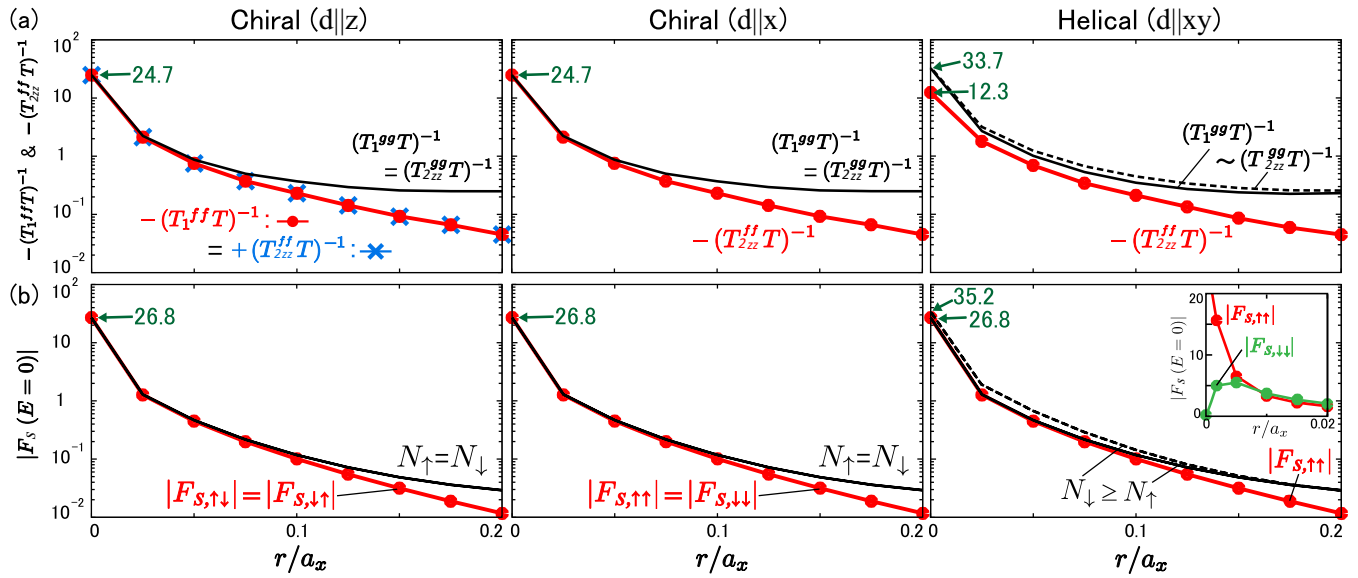

FIG. 4. (a) r dependence of $(T_1^{ff}T)^{-1}$ and $(T_{2zz}^{ff}T)^{-1}$ in the chiral and helical p-wave states. We plot $-(T_1^{ff}T)^{-1}$ and $(T_{2zz}^{ff}T)^{-1}$ for the chiral p-wave $\boldsymbol{d}\|\mathbf{z}$ state, and $-(T_{2zz}^{ff}T)^{-1}$ for the chiral p-wave $\boldsymbol{d}\|\mathbf{x}$ state. These are on the same line. For the helical p-wave state, we plot $-(T_{2zz}^{ff}T)^{-1}$. (b) r dependence of amplitude of odd-frequency s-wave spin-triplet Cooper pairs $|\mathcal{F}_{s,\sigma\sigma'}(E=0,\boldsymbol{r})|$. $|\mathcal{F}_{s,\uparrow\downarrow}(E=0,\boldsymbol{r})| = |\mathcal{F}_{s,\downarrow\uparrow}(E=0,\boldsymbol{r})|$ for the chiral $\boldsymbol{d}\|\mathbf{z}$ state, $|\mathcal{F}_{s,\uparrow\uparrow}(E=0,\boldsymbol{r})| = |\mathcal{F}_{s,\downarrow\downarrow}(E=0,\boldsymbol{r})|$ for the chiral $\boldsymbol{d}\|\mathbf{x}$ state, and $|\mathcal{F}_{s,\uparrow\uparrow}(E=0,\boldsymbol{r})|$ for the helical state show similar r dependence. In the inset, $\mathcal{F}_{s,\downarrow\downarrow}(E=0,\boldsymbol{r})$ for the helical state is suppressed in the vortex core region, compared to $\mathcal{F}_{s,\uparrow\uparrow}(E=0,\boldsymbol{r})$. For comparison, $(T_1^{gg}T)^{-1}$ and $(T_{2zz}^{gg}T)^{-1}$, and $N_\sigma(E=0,\boldsymbol{r})$, for the each state are presented by a black solid line in (a) and (b), respectively.

s-wave Cooper pair is given by

$$\mathcal{F}_{s,\sigma\sigma'}(E,\boldsymbol{r}) = \left\langle \phi_s^*(\boldsymbol{k}) f_{\sigma\sigma'}^R(E,\boldsymbol{r},\boldsymbol{k}) \right\rangle_{\boldsymbol{k}} \tag{18}$$

with the s-wave pairing function $\phi_s(\boldsymbol{k}) = 1$ [10,31]. In the chiral p_--wave superconductor considered in this paper, induced Cooper pair components around a vortex should satisfy the condition $L_z + W = 0$, where L_z is an angular momentum for the induced components of Cooper pairs, and W is a winding number of the component around the vortex. The s-wave component $\mathcal{F}_{s,\sigma\sigma'}(E=0,\boldsymbol{r})$ with $L_z = 0$ has finite amplitude at the vortex center without the phase winding around the vortex ($W = 0$).

In Fig. 4(b), we present the r dependence of the odd-frequency s-wave spin-triplet Cooper pairs around the vortex core. In the chiral p-wave $\boldsymbol{d}\|\mathbf{z}$ state, $(\uparrow,\downarrow)$ and $(\downarrow,\uparrow)$ components are dominant as explained above. On the other hand, in the chiral p-wave $\boldsymbol{d}\|\boldsymbol{x}$ state, the dominant components are $|\mathcal{F}_{s,\uparrow\uparrow}(E=0,\boldsymbol{r})| = |\mathcal{F}_{s,\downarrow\downarrow}(E=0,\boldsymbol{r})|$. In the helical p-wave state, the dominant component is $\mathcal{F}_{s,\uparrow\uparrow}(E=0,\boldsymbol{r})$. These dominant components in the three states have the same r dependence as shown in Fig. 4(b). The amplitude of $\mathcal{F}_{s,\downarrow\downarrow}(E=0,\boldsymbol{r})$ in the helical p-wave state is very small at the vortex core compared to $|\mathcal{F}_{s,\uparrow\uparrow}(E=0,\boldsymbol{r})|$, since induced Cooper pair components in $\Delta_{\downarrow\downarrow}$ satisfy the different condition $L_z + W = 2$, and the amplitude of the induced s-wave component with $L_z = 0$ vanishes at the vortex center due to the phase winding $W = 2$. Therefore, at the vortex center, $|(T_{2zz}^{ff}T)^{-1}|$ in the helical p-wave state indicates the half value ($\simeq$12.3) to $|(T_1^{ff}T)^{-1}|$($\simeq$24.7) in the $\boldsymbol{d}\|\boldsymbol{z}$ state and $|(T_1^{ff}T)^{-1}|$ in the $\boldsymbol{d}\|\boldsymbol{x}$ state.

The finite odd-frequency s-wave spin-triplet Cooper pairs around a vortex core induce the coherence terms. The equal spin components $(\uparrow,\uparrow)$ and $(\downarrow,\downarrow)$ contribute only to T_{2zz}^{-1}. Therefore, $(T_1^{ff}T)^{-1} = 0$ in the two cases of the $\boldsymbol{d}\|\boldsymbol{x}$ state and the helical state. The spin components $(\uparrow,\downarrow)$ and $(\downarrow,\uparrow)$ contribute to both T_1^{-1} and T_{2zz}^{-1}. In the low-temperature limit, from Eq. (B4) in Appendix B, the coherence terms of $(T_1^{ff}T)^{-1}$ and $(T_{2zz}^{ff}T)^{-1}$ are described by the zero-energy amplitude $|\mathcal{F}_{s,\sigma\sigma'}(E=0,\boldsymbol{r})|$ of the odd-frequency s-wave spin-triplet Cooper pair, as $[T_1^{ff}(\boldsymbol{r})T]^{-1} = -|\mathcal{F}_{s,\uparrow\downarrow}(E=0,\boldsymbol{r})|^2$, and $2[T_{2zz}^{ff}(\boldsymbol{r})T]^{-1} = -|\mathcal{F}_{s,\uparrow\uparrow}(E=0,\boldsymbol{r})|^2 - |\mathcal{F}_{s,\downarrow\downarrow}(E=0,\boldsymbol{r})|^2 +$

TABLE I. Relation of the coherence terms with the DOS terms, and existence of the zero-energy odd-frequency s-wave spin-triplet Cooper pairs at the vortex center in the chiral p-wave $\boldsymbol{d}\|\boldsymbol{z}$ and $\boldsymbol{d}\|\boldsymbol{x}$ states, and the helical p-wave state. The value of $|(T_1^{gg}T)^{-1}|$ in the chiral p-wave $\boldsymbol{d}\|\boldsymbol{z}$ state is defined as C.

Main component of	Coherence term		Odd-frequency s-wave spin-triplet Cooper pair
order parameter	$(T_1^{ff}T)^{-1}[\delta M\|z]$	$(T_{2zz}^{ff}T)^{-1}[\delta M\|x]$	$\mathcal{F}_{s,\sigma\sigma'}(E=0,r=0)$
Chiral $\boldsymbol{d}\|\boldsymbol{z}$	$\simeq -(T_1^{gg}T)^{-1} \equiv -C$	$\simeq +(T_{2zz}^{gg}T)^{-1} = +C$	$\|\mathcal{F}_{s,\uparrow\downarrow}\| = \|\mathcal{F}_{s,\downarrow\uparrow}\| \neq 0$
Chiral $\boldsymbol{d}\|\boldsymbol{x}$	$=0$	$\simeq -(T_{2zz}^{gg}T)^{-1} = -C$	$\|\mathcal{F}_{s,\uparrow\uparrow}\| = \|\mathcal{F}_{s,\downarrow\downarrow}\| \neq 0$
Helical ($\boldsymbol{d}\|xy$)	$=0$	$\simeq -C/2$	$\|\mathcal{F}_{s,\uparrow\uparrow}\| \neq 0, \|\mathcal{F}_{s,\downarrow\downarrow}\| = 0$

$|\mathcal{F}_{s,\uparrow\downarrow}(E=0,\boldsymbol{r})|^2+|\mathcal{F}_{s,\downarrow\uparrow}(E=0,\boldsymbol{r})|^2$. Therefore, $(T_{2zz}^{ff}T)^{-1}$ is positive for $\boldsymbol{d}\|\boldsymbol{z}$ with finite $(\uparrow,\downarrow)$ and $(\downarrow,\uparrow)$. And $(T_{2zz}^{ff}T)^{-1}$ is negative in the other two states, since finite components are $(\uparrow,\uparrow)$ and $(\downarrow,\downarrow)$. In the cases of the $\boldsymbol{d}\|\boldsymbol{z}$ state, $\mathcal{F}_{s,\uparrow\uparrow}(E=0,\boldsymbol{r})=\mathcal{F}_{s,\downarrow\downarrow}(E=0,\boldsymbol{r})=0$. In the two cases of the $\boldsymbol{d}\|\boldsymbol{x}$ state and the helical state, $\mathcal{F}_{s,\uparrow\downarrow}(E=0,\boldsymbol{r})=\mathcal{F}_{s,\downarrow\uparrow}(E=0,\boldsymbol{r})=0$.

Since our calculations are performed at the finite temperature $T/T_{c0}=0.5$, the results in Fig. 4 deviate from the relations in the low-T limit in Eq. (B4) by the contribution from finite-energy states, but they satisfy the proportional relations $[T_1^{gg}(\boldsymbol{r})T]^{-1}\propto N(E=0,\boldsymbol{r})^2$, $[T_1^{ff}(\boldsymbol{r})T]^{-1}\propto -|\mathcal{F}_{s,\uparrow\downarrow}(E=0,\boldsymbol{r})|^2$, and also equivalent equations for the $(T_{2zz}T)^{-1}$ case. Therefore, the relation between the DOS term and the coherence term in Table I with C is satisfied. The details of these relations are discussed later in Appendix B.

Lastly, we give some related discussions. In realistic materials such as Sr_2RuO_4, the Fermi surface has multiband nature [1–3]. When multiband superconductivity is realized, the physical quantities are given by the summation of the contributions on the Fermi surfaces of the multibands. Therefore, if the dominant Fermi surfaces have the pair potential with chirality -1 of the chiral p-wave superconductivity, similar anomalous suppression of the local NMR relaxation rates by the negative coherence effects is expected to be observed in the vortex core region. The mechanism that the vortex state of the pair potential with chirality -1 induces the odd-frequency s-wave spin-triplet Cooper pairs and the negative coherence terms is universal, and can be applied to the multiband superconductivity.

Among the possible pairing states of Sr_2RuO_4, there remains a scenario of even-parity spin-singlet pairing [3,32,33]. As for the case of the spin-singlet s-wave or d-wave superconductors, since the odd-frequency s-wave Cooper pairs are not induced at the vortex center, the anomalous suppression of the NMR relaxation rates does not occur [10,34]. Therefore, we can examine the spin components of the pairing, singlet, or triplet, by the site-selective NMR measurements.

In this paper, we do not consider the Zeeman effect. The Zeeman magnetic field will quantitatively affect the NMR relaxation rates in the contribution of the relaxation process between up- and down-spin electrons. And detailed study belongs to future studies. However, when the orbital pair breaking due to the vortex is dominant, the scenario for the anomalous suppression of the NMR relaxation rates due to the odd-frequency Cooper pairs will survive.

V. SUMMARY

We studied the site $\boldsymbol{r}$ and the internal field B dependences of the local NMR relaxation rates T_1^{-1} and T_2^{-1} in the vortex lattice state of chiral p-wave ($\boldsymbol{d}\|\boldsymbol{z}$ or $\boldsymbol{d}\|\boldsymbol{x}$) and helical p-wave superconductors, based on the Eilenberger theory. We focused on how the anomalous suppression of the local T_1^{-1} and T_2^{-1} around the vortex core reflects the d-vector symmetry of the pair potential. The anomalous suppression occurs by the negative coherence term coming from the odd-frequency s-wave spin-triplet Cooper pairs $\mathcal{F}_{s,\sigma\sigma'}$. The finite spin $(\sigma\sigma')$ components of $\mathcal{F}_{s,\sigma\sigma'}$ reflect the d-vector orientation, and determine in which of T_1^{-1} and T_2^{-1} the anomalous suppression occurs. Since the anomalous suppression can be observed when the NMR relaxation direction δM is parallel to the d-vector component, we may obtain the information of the d-vector symmetry by comparative observation of the local T_1^{-1} and T_2^{-1} at the vortex core region in the site-selective NMR measurement. In the chiral p-wave $\boldsymbol{d}\|\boldsymbol{z}$ ($\boldsymbol{d}\|\boldsymbol{x}$) state, since the odd-frequency s-wave spin-triplet Cooper pairs $\mathcal{F}_{s,\uparrow\downarrow(\uparrow\uparrow)}$ and $\mathcal{F}_{s,\downarrow\uparrow(\downarrow\downarrow)}$ are induced around the vortex core, the anomalous suppression in the local T_1^{-1} (T_2^{-1}) occurs. In the helical p-wave state, since the odd-frequency s-wave spin-triplet Cooper pairs $\mathcal{F}_{s,\uparrow\uparrow}$ are only induced, the difference between the local T_1^{-1} and T_2^{-1} is small. We hope that these theoretical results of the local NMR relaxation rates will be examined by experiment in spin-triplet superconductors. This observation can be also a method to detect the spin dependence of the odd-frequency s-wave spin-triplet Cooper pairs.

ACKNOWLEDGMENT

This work was supported by Japan Society for the Promotion of Science KAKENHI Grant No. JP16J05824.

APPENDIX A: NMR RELAXATION RATES T_1^{-1} AND T_2^{-1}

We explain derivations of the NMR relaxation rates T_1^{-1} and T_2^{-1} in the quasiclassical Eilenberger theory. In the 4×4 matrix form for the Green's functions

$$\check{G}(x,x')=\begin{bmatrix}\hat{G}(x,x') & \hat{F}(x,x')\\ \hat{\bar{F}}(x,x') & \hat{\bar{G}}(x,x')\end{bmatrix} \tag{A1}$$

in particle-hole and spin spaces, the spin components of $\hat{G}$, $\hat{F}$, $\hat{\bar{F}}$, and $\hat{\bar{G}}$ are, respectively, defined as

$$\begin{aligned}G_{\sigma\sigma'}(x,x')&=-\langle T_\tau[\psi_\sigma(x)\psi_{\sigma'}^\dagger(x')]\rangle,\\ \bar{G}_{\sigma\sigma'}(x,x')&=-\langle T_\tau[\psi_\sigma^\dagger(x)\psi_{\sigma'}(x')]\rangle,\\ F_{\sigma\sigma'}(x,x')&=-\langle T_\tau[\psi_\sigma(x)\psi_{\sigma'}(x')]\rangle,\\ \bar{F}_{\sigma\sigma'}(x,x')&=-\langle T_\tau[\psi_\sigma^\dagger(x)\psi_{\sigma'}^\dagger(x')]\rangle,\end{aligned} \tag{A2}$$

where $x=(\boldsymbol{r},\tau)$ with the coordinate $\boldsymbol{r}$ and imaginary time τ. The brackets $\langle\cdots\rangle$ denote the thermal average, and T_τ is the time-ordering operator. In the Eilenberger theory, the quasiclassical Green's function is defined as $\check{g}=\check{\tau}_3\int d\xi_k\check{G}$, where $\xi_k=\epsilon(\boldsymbol{k})-\mu$ is the energy variable in the k space. $\epsilon(\boldsymbol{k})$ is the dispersion relation of electrons, and μ is the chemical potential. $\check{\tau}_3$ is the Pauli matrix defined as

$$\check{\tau}_3=\begin{bmatrix}\hat{\sigma}_0 & \hat{0}\\ \hat{0} & -\hat{\sigma}_0\end{bmatrix}, \tag{A3}$$

where $\hat{\sigma}_0$ is the unit matrix. In Appendix A, we write the matrix components of $\check{g}$ as

$$\check{g}=\begin{bmatrix}\hat{g}^{11} & \hat{g}^{12}\\ \hat{g}^{21} & \hat{g}^{22}\end{bmatrix}, \tag{A4}$$

instead of the expression in Eq. (3).

The spin-lattice relaxation rate T_1^{-1} is obtained from the spin-spin correlation function

$$\chi_{-+}(x,x') = \langle T_\tau[S_-(x)S_+(x')]\rangle = \bar{G}_{\downarrow\downarrow}(x,x')G_{\uparrow\uparrow}(x,x') - \bar{F}_{\downarrow\uparrow}(x,x')F_{\uparrow\downarrow}(x,x'), \tag{A5}$$

where

$$S_-(x) = \psi_\downarrow^\dagger(x)\psi_\uparrow(x), \quad S_+(x) = \psi_\uparrow^\dagger(x)\psi_\downarrow(x). \tag{A6}$$

The Fourier transformation of χ_{-+} is

$$\chi_{-+}(\boldsymbol{r},\boldsymbol{r}';i\Omega_m) = \int_0^\beta d\tau e^{i\Omega_m\tau}\chi_{-+}(\boldsymbol{r},\boldsymbol{r}';\tau) \tag{A7}$$

$$= \int_0^\beta d\tau e^{i\Omega_m\tau}[\bar{G}_{\downarrow\downarrow}(\boldsymbol{r},\boldsymbol{r}';\tau)G_{\uparrow\uparrow}(\boldsymbol{r},\boldsymbol{r}';\tau) - \bar{F}_{\downarrow\uparrow}(\boldsymbol{r},\boldsymbol{r}';\tau)F_{\uparrow\downarrow}(\boldsymbol{r},\boldsymbol{r}';\tau)] \tag{A8}$$

$$= \frac{1}{\beta}\sum_{\omega_n}[\bar{G}_{\downarrow\downarrow}(\boldsymbol{r},\boldsymbol{r}';i\omega_n)G_{\uparrow\uparrow}(\boldsymbol{r},\boldsymbol{r}';i\Omega_m - i\omega_n) - \bar{F}_{\downarrow\uparrow}(\boldsymbol{r},\boldsymbol{r}';i\omega_n)F_{\uparrow\downarrow}(\boldsymbol{r},\boldsymbol{r}';i\Omega_m - i\omega_n)] \tag{A9}$$

with Bose-Matsubara frequency Ω_m and $\beta \equiv (k_B T)^{-1}$.

For the quasiclassical approximation as done in Refs. [8,9,34,35], in the limit $\boldsymbol{r} \to \boldsymbol{r}'$ the Green's functions are rewritten using the transformation

$$A(\boldsymbol{r},\boldsymbol{r}) = \lim_{\bar{\boldsymbol{r}}\to 0}\int\frac{d^3k}{(2\pi)^3}A(\boldsymbol{r},\boldsymbol{k})e^{i\boldsymbol{k}\bar{\boldsymbol{r}}} \tag{A10}$$

$$\approx N_0\left\langle\int d\xi_k A(\boldsymbol{r},\boldsymbol{k}_F,\xi_k)\right\rangle_{\boldsymbol{k}_F}, \tag{A11}$$

with $\bar{\boldsymbol{r}} \equiv \boldsymbol{r} - \boldsymbol{r}'$. In the following, for simplicity, we rewrite the Fermi velocity $\boldsymbol{k}_F \to \boldsymbol{k}$. Therefore, the quasiclassical form of the local χ_{-+} is written as

$$\chi_{-+}(\boldsymbol{r},\boldsymbol{r};i\Omega_m) = N_0^2\frac{1}{\beta}\sum_{\omega_n}[\langle g_{\downarrow\downarrow}^{22}(i\omega_n,\boldsymbol{r},\boldsymbol{k})\rangle_{\boldsymbol{k}}\langle g_{\uparrow\uparrow}^{11}(i\Omega_m - i\omega_n,\boldsymbol{r},\boldsymbol{k})\rangle_{\boldsymbol{k}} - \langle g_{\downarrow\uparrow}^{21}(i\omega_n,\boldsymbol{r},\boldsymbol{k})\rangle_{\boldsymbol{k}}\langle g_{\uparrow\downarrow}^{12}(i\Omega_m - i\omega_n,\boldsymbol{r},\boldsymbol{k})\rangle_{\boldsymbol{k}}]. \tag{A12}$$

Using the spectral representation

$$g_{\sigma\sigma'}^{ij}(i\omega_n,\boldsymbol{r},\boldsymbol{k}) = \int_{-\infty}^{\infty}d\omega\frac{a_{\sigma\sigma'}^{ij}(\omega,\boldsymbol{r},\boldsymbol{k})}{i\omega_n - \omega} \tag{A13}$$

and an analytic continuation $i\Omega_m \to \Omega + i\delta$, we obtain the local spin-lattice relaxation rate T_1^{-1} as

$$T_1^{-1}(\boldsymbol{r},T) = T\lim_{\Omega\to 0}\mathrm{Im}\frac{\chi_{-+}(\boldsymbol{r},\boldsymbol{r},i\Omega_m\to\Omega+i\delta)}{\Omega} = \frac{\pi N_0^2}{4}\int_{-\infty}^{\infty}dE\frac{1}{\cosh^2(E/2T)} \times [\langle a_{\downarrow\downarrow}^{22}(E)\rangle_{\boldsymbol{k}}\langle a_{\uparrow\uparrow}^{11}(-E)\rangle_{\boldsymbol{k}} - \langle a_{\downarrow\uparrow}^{21}(E)\rangle_{\boldsymbol{k}}\langle a_{\uparrow\downarrow}^{12}(-E)\rangle_{\boldsymbol{k}}]. \tag{A14}$$

$a_{\sigma\sigma'}^{ij}$ is shown in Eq. (12). Since $T_1^{-1} = \pi T_c N_0^2$ at $T = T_c$, we obtain $[T_1(T)T]^{-1}/[T_1(T_c)T_c]^{-1}$ in Eq. (9).

On the other hand, we calculate the z-component T_{2zz}^{-1} of the spin-spin relaxation rate T_2^{-1} from the dynamical spin susceptibility χ_{zz}, given by

$$4\chi_{zz}(x,x') = 4\langle T_\tau[S_z(x)S_z(x')]\rangle = \bar{G}_{\uparrow\uparrow}(x,x')G_{\uparrow\uparrow}(x,x') - \bar{F}_{\uparrow\uparrow}(x,x')F_{\uparrow\uparrow}(x,x') + \bar{G}_{\downarrow\downarrow}(x,x')G_{\downarrow\downarrow}(x,x') - \bar{F}_{\downarrow\downarrow}(x,x')F_{\downarrow\downarrow}(x,x') - \bar{G}_{\uparrow\downarrow}(x,x')G_{\uparrow\downarrow}(x,x') + \bar{F}_{\uparrow\downarrow}(x,x')F_{\uparrow\downarrow}(x,x') - \bar{G}_{\downarrow\uparrow}(x,x')G_{\downarrow\uparrow}(x,x') + \bar{F}_{\downarrow\uparrow}(x,x')F_{\downarrow\uparrow}(x,x') = \sum_{\sigma\sigma'}S_{\sigma\sigma'}[\bar{G}_{\sigma\sigma'}(x,x')G_{\sigma\sigma'}(x,x') - \bar{F}_{\sigma\sigma'}(x,x')F_{\sigma\sigma'}(x,x')], \tag{A15}$$

where

$$2S_z(x) = \psi_\uparrow^\dagger(x)\psi_\uparrow(x) - \psi_\downarrow^\dagger(x)\psi_\downarrow(x). \tag{A16}$$

Therefore,

$$\frac{1}{2}T_{2zz}^{-1}(\boldsymbol{r},T) = T\lim_{\Omega\to 0}\mathrm{Im}\frac{\chi_{zz}(\boldsymbol{r},\boldsymbol{r},i\Omega_m\to\Omega+i\delta)}{\Omega} \tag{A17}$$

is calculated as in the similar methods to the derivation of T_1^{-1}, and we obtain $[T_{2zz}(T)T]^{-1}/[T_{2zz}(T_c)T_c]^{-1}$ in Eq. (14).

APPENDIX B: BEHAVIORS OF T_1^{-1} AND T_2^{-1} IN THE LOW-TEMPERATURE LIMIT

In the limit of low temperature $T \to 0$, T_1^{-1} in Eq. (9) and T_2^{-1} in Eq. (14) are, respectively, reduced to

$$\frac{[T_1(\boldsymbol{r})T]^{-1}}{[T_1(T_c)T_c]^{-1}} = W_{sl}^{gg}(E=0,\boldsymbol{r}) + W_{sl}^{ff}(E=0,\boldsymbol{r}), \tag{B1}$$

$$2\frac{[T_{2zz}(\boldsymbol{r})T]^{-1}}{[T_{2zz}(T_c)T_c]^{-1}} = \sum_{\sigma\sigma'}S_{\sigma\sigma'}\big[W_{\sigma\sigma'}^{gg}(E=0,\boldsymbol{r}) + W_{\sigma\sigma'}^{ff}(E=0,\boldsymbol{r})\big]. \tag{B2}$$

These indicate that the zero-energy contribution is dominant at $T \to 0$.

Using the following relations, we obtain the relations for the zero-energy excitations and the odd-frequency spin-triplet Cooper pairs from Eq. (12). Between advanced and retarded Green's functions, there are relations $g_{\sigma\sigma'}^R(E) = -g_{\sigma'\sigma}^{A*}(E)$ and $\bar{f}_{\sigma\sigma'}^R(E) = f_{\sigma'\sigma}^{A*}(E)$. From the parity in the E dependence of odd-frequency spin-triplet Cooper pairs, $\bar{f}_{\sigma\sigma'}^R(E) = -f_{\sigma'\sigma}^{R*}(-E)$. In addition, in the spin-triplet superconducting state without Zeeman effects, $g_{\uparrow\downarrow}^R(E) = g_{\downarrow\uparrow}^R(E) = 0$ and $f_{\uparrow\downarrow}^R(E) = f_{\downarrow\uparrow}^R(E)$. In the limit $E \to 0$, we obtain

$$a_{\sigma\sigma'}^{11}(E,\boldsymbol{r},\boldsymbol{k}) = \frac{1}{2}\big[g_{\sigma\sigma'}^R(E,\boldsymbol{r},\boldsymbol{k}) + g_{\sigma'\sigma}^{R*}(E,\boldsymbol{r},\boldsymbol{k})\big] = \frac{1}{2}\big[g_{\sigma\sigma'}^R(E,\boldsymbol{r},\boldsymbol{k}) + g_{\sigma\sigma'}^{R*}(E,\boldsymbol{r},\boldsymbol{k})\big] \to \mathrm{Re}\big[g_{\sigma\sigma'}^R(E=0,\boldsymbol{r},\boldsymbol{k})\big]\delta_{\sigma\sigma'},$$

$$
\begin{aligned}
a^{22}_{\sigma\sigma'}(E,\boldsymbol{r},\boldsymbol{k}) &= \frac{1}{2}\left[\bar{g}^R_{\sigma\sigma'}(E,\boldsymbol{r},\boldsymbol{k}) + \bar{g}^{R*}_{\sigma'\sigma}(E,\boldsymbol{r},\boldsymbol{k})\right] \\
&= \frac{1}{2}\left[\bar{g}^R_{\sigma\sigma'}(E,\boldsymbol{r},\boldsymbol{k}) + \bar{g}^{R*}_{\sigma\sigma'}(E,\boldsymbol{r},\boldsymbol{k})\right] \\
&\to \mathrm{Re}\left[\bar{g}^R_{\sigma\sigma'}(E=0,\boldsymbol{r},\boldsymbol{k})\right]\delta_{\sigma\sigma'}, \\
a^{12}_{\sigma\sigma'}(E,\boldsymbol{r},\boldsymbol{k}) &= \frac{i}{2}\left[f^R_{\sigma\sigma'}(E,\boldsymbol{r},\boldsymbol{k}) - \bar{f}^{R*}_{\sigma'\sigma}(E,\boldsymbol{r},\boldsymbol{k})\right] \\
&= \frac{i}{2}\left[f^R_{\sigma\sigma'}(E,\boldsymbol{r},\boldsymbol{k}) + f^R_{\sigma\sigma'}(-E,\boldsymbol{r},\boldsymbol{k})\right] \\
&\to \mathrm{i} f^R_{\sigma\sigma'}(E=0,\boldsymbol{r},\boldsymbol{k}), \\
a^{21}_{\sigma\sigma'}(E,\boldsymbol{r},\boldsymbol{k}) &= \frac{i}{2}\left[\bar{f}^R_{\sigma\sigma'}(E,\boldsymbol{r},\boldsymbol{k}) - f^{R*}_{\sigma'\sigma}(E,\boldsymbol{r},\boldsymbol{k})\right] \\
&= -\frac{i}{2}\left[f^{R*}_{\sigma'\sigma}(-E,\boldsymbol{r},\boldsymbol{k}) + f^{R*}_{\sigma'\sigma}(E,\boldsymbol{r},\boldsymbol{k})\right] \\
&\to -\mathrm{i} f^{R*}_{\sigma\sigma'}(E=0,\boldsymbol{r},\boldsymbol{k}), \qquad \text{(B3)}
\end{aligned}
$$

where $\delta_{\sigma\sigma'}=1$ when $\sigma=\sigma'$ and $\delta_{\sigma\sigma'}=0$ when $\sigma\neq\sigma'$. Therefore, in the low-energy limit, the DOS term and the coherence term of $(T_1T)^{-1}$ and $(T_{2zz}T)^{-1}$ in the vortex core region are, respectively, reduced to

$$
\begin{aligned}
\frac{\left[T_1^{gg}(T)T\right]^{-1}}{[T_1(T_c)T_c]^{-1}} &= \langle \mathrm{Re}[\bar{g}^R_{\downarrow\downarrow}(E=0)]\rangle_{\boldsymbol{k}}\langle \mathrm{Re}[g^R_{\uparrow\uparrow}(E=0)]\rangle_{\boldsymbol{k}} \\
&= N_\downarrow(E=0)N_\uparrow(E=0), \\
\frac{\left[T_1^{ff}(T)T\right]^{-1}}{[T_1(T_c)T_c]^{-1}} &= -|\langle f^R_{\uparrow\downarrow}(E=0)\rangle_{\boldsymbol{k}}|^2 = -|\mathcal{F}_{s,\uparrow\downarrow}(E=0)|^2 \\
&= -|\langle f^R_{\downarrow\uparrow}(E=0)\rangle_{\boldsymbol{k}}|^2 = -|\mathcal{F}_{s,\downarrow\uparrow}(E=0)|^2, \\
2\frac{\left[T_{2zz}^{gg}(T)T\right]^{-1}}{[T_{2zz}(T_c)T_c]^{-1}} &= \sum_{\sigma\sigma'}\delta_{\sigma\sigma'}\left\langle \mathrm{Re}\left[g^R_{\sigma\sigma'}(E=0)\right]\right\rangle^2_{\boldsymbol{k}} \\
&= N_\uparrow(E=0)^2 + N_\downarrow(E=0)^2, \\
2\frac{\left[T_{2zz}^{ff}(T)T\right]^{-1}}{[T_{2zz}(T_c)T_c]^{-1}} &= -\sum_{\sigma\sigma'}S_{\sigma\sigma'}\left|\left\langle f^R_{s,\sigma\sigma'}(E=0)\right\rangle_{\boldsymbol{k}}\right|^2 \\
&= -\sum_{\sigma\sigma'}S_{\sigma\sigma'}|\mathcal{F}_{s,\sigma\sigma'}(E=0)|^2, \qquad \text{(B4)}
\end{aligned}
$$

where $\hat{\bar{g}}^R(E,\boldsymbol{r},\boldsymbol{k}) = \hat{g}^R(-E,\boldsymbol{r},\boldsymbol{k})$, and Eqs. (17) and (18) are used.

Further, in the low-energy limit at low T and the limit of a single vortex at low H, in the chiral p-wave $\boldsymbol{d}\|\boldsymbol{z}$ state we have the relations $|\langle g^R_{\sigma\sigma}(E)\rangle_{\boldsymbol{k}}| = |\langle f^R_{\sigma\sigma'}(E)\rangle_{\boldsymbol{k}}| = |\langle \bar{f}^R_{\sigma\sigma'}(E)\rangle_{\boldsymbol{k}}|$ with $\sigma\neq\sigma'$ by the Kramer-Pesch approximation for low-energy states [36,37]. Then, we obtain the relation for the coherence terms as

$$
\frac{\left[T_1^{ff}(T)T\right]^{-1}}{[T_1(T_c)T_c]^{-1}} = -\frac{\left[T_1^{gg}(T)T\right]^{-1}}{[T_1(T_c)T_c]^{-1}}, \qquad \text{(B5)}
$$

$$
\frac{\left[T_{2zz}^{ff}(T)T\right]^{-1}}{\left[T_{2zz}(T_c)T_c\right]^{-1}} = \frac{\left[T_{2zz}^{gg}(T)T\right]^{-1}}{[T_1(T_c)T_c]^{-1}}, \qquad \text{(B6)}
$$

at the vortex core region, since $|\langle f^R_{\uparrow\downarrow}(E=0)\rangle_{\boldsymbol{k}}| = |\langle f^R_{\downarrow\uparrow}(E=0)\rangle_{\boldsymbol{k}}|\neq 0$. In the chiral p-wave $\boldsymbol{d}\|\boldsymbol{x}$ state, using the relations $|\langle g^R_{\sigma\sigma}(E)\rangle_{\boldsymbol{k}}| = |\langle f^R_{\sigma\sigma}(E)\rangle_{\boldsymbol{k}}| = |\langle \bar{f}^R_{\sigma\sigma}(E)\rangle_{\boldsymbol{k}}|$ given by the Kramer-Pesch approximation, we obtain

$$
\frac{\left[T_{2zz}^{ff}(T)T\right]^{-1}}{[T_{2zz}(T_c)T_c]^{-1}} = -\frac{\left[T_{2zz}^{gg}(T)T\right]^{-1}}{[T_1(T_c)T_c]^{-1}}, \qquad \text{(B7)}
$$

since $|\langle f^R_{\uparrow\uparrow}(E=0)\rangle_{\boldsymbol{k}}| = |\langle f^R_{\downarrow\downarrow}(E=0)\rangle_{\boldsymbol{k}}|\neq 0$. These relations for the chiral p-wave states in Eqs. (B5)–(B7) are consistent with the calculation results of the negative coherence terms in the vortex core region at finite temperature and magnetic field in Fig. 4(a) and Table I.

In addition, up-spin pairs and excitations in the helical p-wave state satisfy the relations $|\langle g^R_{\uparrow\uparrow}(E)\rangle_{\boldsymbol{k}}| = |\langle f^R_{\uparrow\uparrow}(E)\rangle_{\boldsymbol{k}}| = |\langle \bar{f}^R_{\uparrow\uparrow}(E)\rangle_{\boldsymbol{k}}|$ given by the Kramer-Pesch approximation, since up-spin pairs' order parameter $\Delta_{\uparrow\uparrow}$ has the pairing function ϕ_{p_-} with the chirality $L_z=-1$ [27]. On the other hand, $|\langle f^R_{\downarrow\downarrow}(E=0)\rangle_{\boldsymbol{k}}| = 0$ at the vortex center. Therefore, in the helical p-wave state,

$$
\begin{aligned}
2\frac{\left[T_{2zz}^{ff}(T)T\right]^{-1}}{[T_{2zz}(T_c)T_c]^{-1}} &= -|\langle g^R_{\uparrow\uparrow}(E=0)\rangle_{\boldsymbol{k}}|^2 - |\langle f^R_{\downarrow\downarrow}(E=0)\rangle_{\boldsymbol{k}}|^2 \\
&= -N_\uparrow(E=0)^2 - |\langle f^R_{\downarrow\downarrow}(E=0)\rangle_{\boldsymbol{k}}|^2 \\
&\sim -N_\uparrow(E=0)^2, \qquad \text{(B8)}
\end{aligned}
$$

since $|\langle f^R_{\downarrow\downarrow}(E=0)\rangle_{\boldsymbol{k}}|$ shows a small amplitude in the vortex core region compared to the large amplitude $|\langle f^R_{\uparrow\uparrow}(E=0)\rangle_{\boldsymbol{k}}|$.

From the definitions of the local DOS $N_\sigma(E,\boldsymbol{r}) = \langle \mathrm{Re}[g^R_{\sigma\sigma}(E,\boldsymbol{r},\boldsymbol{k})]\rangle_{\boldsymbol{k}}$ and the spin-dependent s-wave Cooper pair $\mathcal{F}_{s,\sigma\sigma'}(E,\boldsymbol{r}) = \langle f^R_{\sigma\sigma'}(E,\boldsymbol{r},\boldsymbol{k})\rangle_{\boldsymbol{k}}$, the relations between the $|\langle g_{\sigma\sigma'}(E)\rangle|$ and $|\langle f_{\sigma\sigma'}(E)\rangle|$ obtained from Kramer-Pesch approximation are rewritten by $N_\sigma(E,\boldsymbol{r})$ and $|\mathcal{F}_{s,\sigma\sigma'}(E,\boldsymbol{r})|$. As shown in Fig. 5(a), the relation $|\langle g^R_{\uparrow\uparrow}(E)\rangle_{\boldsymbol{k}}| = |\langle f^R_{\uparrow\uparrow}(E)\rangle_{\boldsymbol{k}}|$, i.e., $|\mathcal{F}_{s,\uparrow\uparrow}(E,\boldsymbol{r}=0)| = |N_\uparrow(E,\boldsymbol{r}=0)|$, for the helical p-wave state is confirmed at the low $|E|$ region, not only $E=0$, by our numerical calculations at a low field $H/H_{c2}=0.023$ and a finite temperature $T/T_{c0}=0.5$. The chiral p-wave cases are also confirmed. Therefore, the relations between the DOS

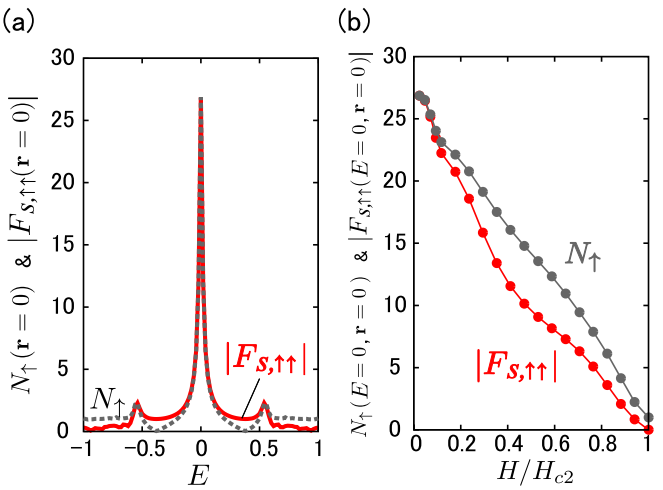

FIG. 5. (a) E dependence of $|\mathcal{F}_{s,\uparrow\uparrow}(\boldsymbol{r}=0)|$ and $|N_\uparrow(\boldsymbol{r}=0)|$ at the vortex center for the helical p-wave states. $H/H_{c2}\simeq 0.023$ and $T/T_{c0}=0.5$. (b) H dependence of $|\mathcal{F}_{s,\uparrow\uparrow}(E=0,\boldsymbol{r}=0)|$ and $|N_\uparrow(E=0,\boldsymbol{r}=0)|$ at the vortex center for the helical p-wave states. $T/T_{c0}=0.5$.

term and the coherence term for the chiral p-wave states in Eqs. (B5)–(B7) are consistent with our calculation results in Fig. 4 and Table I. Due to the contributions from finite energies $N_\sigma(E,\boldsymbol{r})$ and $|\mathcal{F}_{s,\sigma\sigma'}(E,\boldsymbol{r})|$, the results in Fig. 4 at finite temperature deviate from Eq. (B8) from the relations Eq. (B4) in the low-T limit.

In addition, Fig. 5(b) shows that the condition $|N_\uparrow(E = 0,\boldsymbol{r} = 0)| = |\mathcal{F}_{s,\uparrow\uparrow}(E = 0,\boldsymbol{r} = 0)|$ is sustained at finite H, while small deviations from the relation appear with increasing H. B dependences of the local T_1^{-1} in the chiral p-wave $\boldsymbol{d}\|\boldsymbol{z}$ states at various applied fields are investigated in a previous study [10].

[1] A. P. Mackenzie and Y. Maeno, Rev. Mod. Phys. **75**, 657 (2003).
[2] Y. Maeno, S. Kittaka, T. Nomura, S. Yonezawa, and K. Ishida, J. Phys. Soc. Jpn. **81**, 011009 (2012).
[3] A. P. Mackenzie, T. Scaffidi, C. W. Hicks, and Y. Maeno, NPJ Quantum Mater. **2**, 40 (2017).
[4] H. Tou, Y. Kitaoka, K. Asayama, N. Kimura, Y. Ōnuki, E. Yamamoto, and K. Maezawa, Phys. Rev. Lett. **77**, 1374 (1996).
[5] H. Tou, Y. Kitaoka, K. Ishida, K. Asayama, N. Kimura, Y. Onuki, E. Yamamoto, Y. Haga, and K. Maezawa, Phys. Rev. Lett. **80**, 3129 (1998).
[6] M. J. Graf, S. K. Yip, and J. A. Sauls, Phys. Rev. B **62**, 14393 (2000).
[7] M. Takigawa, M. Ichioka, K. Machida, and M. Sigrist, J. Phys.: Chem. Solids **63**, 1333 (2002).
[8] N. Hayashi and Y. Kato, Physica C **388**, 513 (2003); J. Low Temp. Phys. **131**, 893 (2003).
[9] Y. Kato and N. Hayashi, Physica C **388**, 519 (2003).
[10] K. K. Tanaka, M. Ichioka, and S. Onari, Phys. Rev. B **93**, 094507 (2016).
[11] N. J. Curro, C. Milling, J. Haase, and C. P. Slichter, Phys. Rev. B **62**, 3473 (2000).
[12] V. F. Mirtović, E. E. Sigmund, M. Eschrig, H. N. Bachman, W. P. Halperin, A. P. Reyes, P. Kuhns, and W. G. Moulton, Nature (London) **413**, 501 (2001).
[13] K. Kakuyanagi, K.-i. Kumagai, and Y. Matsuda, Phys. Rev. B **65**, 060503(R) (2002); K. Kakuyanagi, K. Kumagai, Y. Matsuda, and M. Hasegawa, Phys. Rev. Lett. **90**, 197003 (2003).
[14] Y. Nakai, Y. Hayashi, K. Kitagawa, K. Ishida, H. Sugawara, D. Kikuchi, and H. Sato, J. Phys. Soc. Jpn. **77**, 333 (2008); Y. Nakai, Y. Hayashi, K. Ishida, H. Sugawara, D. Kikuchi, and H. Sato, Physica B **403**, 1109 (2008).
[15] C. M. Aegerter, S. H. Lloyd, C. Ager, S. L. Lee, S. Romer, H. Keller, and E. M. Forgan, J. Phys.: Condens. Matter **10**, 7445 (1998).
[16] V. Kozil, J. W. F. Venderbos, and L. Fu, Sci. Adv. **2**, e1601835 (2016).
[17] T. Mizushima, Phys. Rev. B **90**, 184506 (2014).
[18] S. B. Chung and S. C. Zhang, Phys. Rev. Lett. **103**, 235301 (2009).
[19] Y. Asano and Y. Tanaka, Phys. Rev. B **87**, 104513 (2013).
[20] S. Higashitani, S. Matsuo, Y. Nagato, K. Nagai, S. Murakawa, R. Nomura, and Y. Okuda, Phys. Rev. B **85**, 024524 (2012).
[21] Y. Tsutsumi and K. Machida, J. Phys. Soc. Jpn. **81**, 074607 (2012).
[22] H.-Y. Hui, J. D. Sau, and S. Das Sarma, Phys. Rev. B **90**, 064516 (2014).
[23] F. Bloch, Phys. Rev. **70**, 460 (1946).
[24] R. K. Wangsness and F. Bloch, Phys. Rev. **89**, 728 (1953).
[25] T. Moriya, J. Phys. Soc. Jpn. **18**, 516 (1963).
[26] Y. Tsutsumi, T. Kawakami, K. Shiozaki, M. Sato, and K. Machida, Phys. Rev. B **91**, 144504 (2015).
[27] K. K. Tanaka, M. Ichioka, and S. Onari, Phys. Rev. B **95**, 134502 (2017).
[28] R. Heeb and D. F. Agterberg, Phys. Rev. B **59**, 7076 (1999).
[29] M. Ichioka and K. Machida, Phys. Rev. B **65**, 224517 (2002).
[30] T. Daino, M. Ichioka, T. Mizushima, and Y. Tanaka, Phys. Rev. B **86**, 064512 (2012).
[31] Y. Tanuma, N. Hayashi, Y. Tanaka, and A. A. Golubov, Phys. Rev. Lett. **102**, 117003 (2009).
[32] K. Machida and M. Ichioka, Phys. Rev. B **77**, 184515 (2008).
[33] Y. Amano, M. Ishihara, M. Ichioka, N. Nakai, and K. Machida, Phys. Rev. B **91**, 144513 (2015).
[34] K. K. Tanaka, M. Ichioka, S. Onari, N. Nakai, and K. Machida, Phys. Rev. B **91**, 014509 (2015).
[35] Y. Nagai, N. Hayashi, N. Nakai, H. Nakamura, M. Okumura, and M. Machida, New J. Phys. **10**, 103026 (2008).
[36] L. Kramer and W. Pesch, Z. Phys. **269**, 59 (1974).
[37] Y. Kato and N. Hayashi, J. Phys. Soc. Jpn. **70**, 3368 (2001); **71**, 1721 (2002).